Heliyon 9 (2023) e21676

Contents lists available at ScienceDirect

Heliyon

journal homepage: www.cell.com/heliyon

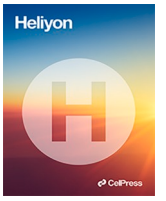

Copine7 deficiency leads to hepatic fat accumulation via mitochondrial dysfunction

Geumbit Hwang [a,b], Hyejin Seo [a], Joo-Cheol Park [a,b,*]

[a] Laboratory for the Study of Regenerative Dental Medicine, Department of Oral Histology-Developmental Biology & Dental Research Institute, School of Dentistry, Seoul National University, Seoul, Republic of Korea
[b] Regenerative Dental Medicine R & D Center, HysensBio, Co., Ltd., 10 Dwitgol-ro, Gwacheon-si, Gyeonggi-do, Republic of Korea

ARTICLE INFO

Keywords:
Copine7
fatty liver
Reactive oxygen species
Lipid metabolism
Mitochondrial dynamics

ABSTRACT

Objective: Mitochondrial dysfunction affects hepatic lipid homeostasis and promotes ROS generation. Copine7 (CPNE7) belongs to the ubiquitous copine family of calcium-dependent phospholipid binding proteins. CPNE7 has a high calcium ion binding affinity and the capacity to scavenge reactive oxygen species (ROS). A recent study reported that abnormalities in fatty acid and lipid metabolism were linked to the gene variant of CPNE7. Therefore, the purpose of this study is to examine the role of Cpne7 in hepatic lipid metabolism based on mitochondrial function.

Methods: Lipid metabolism, mitochondrial function, and ROS production were investigated in high-fat diet (HFD)-fed *Cpne7*$^{-/-}$ mice and H_2O_2-damaged HepG2 hepatocytes following *CPNE7* silencing or overexpression.

Results: Cpne7 deficiency promoted severe hepatic steatosis in the HFD-induced NAFLD model. More importantly, mitochondrial dysfunction was observed along with an imbalance of mitochondrial dynamics in the livers of HFD-fed *Cpne7*$^{-/-}$mice, resulting in high ROS levels. Similarly, *CPNE7*-silenced HepG2 hepatocytes showed high ROS levels, mitochondrial dysfunction, and increased lipid contents. On the contrary, *CPNE7*-overexpressed HepG2 cells showed low ROS levels, enhanced mitochondrial function and decreased lipid contents under H_2O_2-induced oxidative stress.

Conclusions: In the liver, *Cpne7* deficiency causes excessive ROS formation and mitochondrial dysfunction, which aggravates lipid metabolism abnormalities. These findings provide evidence that *Cpne7* deficiency contributes to the pathogenesis of NAFLD, suggesting *Cpne7* as a novel therapeutic target for NAFLD.

1. Introduction

Mitochondria are essential organelles that play a vital roles in cell biology by producing energy through fatty acid beta-oxidation, the tricarboxylic acid cycle, and oxidative phosphorylation [1]. Metabolic stressors or genetic variants can be responsible for mitochondrial dysfunction. Mitochondrial dysfunction is primarily characterized by excessive ROS formation, oxidative stress, and reduced respiratory chain. These results are intimately linked to lipid accumulation, inflammation, and hepatic cell death during the

* Corresponding author. Laboratory for the Study of Regenerative Dental Medicine, Department of Oral Histology and Developmental Biology, School of Dentistry, Seoul National University, 1 Gwanak-ro, Gwanak-gu, Seoul, 08826, Republic of Korea.
E-mail address: jcapark@snu.ac.kr (J.-C. Park).

https://doi.org/10.1016/j.heliyon.2023.e21676
Received 14 August 2023; Received in revised form 25 October 2023; Accepted 25 October 2023
Available online 28 October 2023

non-alcoholic fatty liver disease (NAFLD) development [2]. Therefore, NAFLD is also regarded as a form of mitochondrial disease [3].

NAFLD, a chronic liver disorder, is one of the most prevalent metabolic diseases and a public health concern worldwide [4,5]. However, there is no approved treatment for NAFLD to date. Therefore, it is necessary to better understand the pathological mechanism of NAFLD and to develop therapeutic targets. NAFLD is mainly characterized by lipid metabolic disorder, and hepatic lipid is produced by the influx of fatty acids through *de novo* lipogenesis, adipose tissue lipolysis, and reabsorption in circulation [6,7]. Hepatic lipids are removed through the beta-oxidation of fatty acids in mitochondria and their release into very-low-density lipoprotein (VLDL) [8]. The liver is one of the most mitochondrial-rich tissues, and there are between 500 and 4000 mitochondria per hepatocyte [9]. During early stages of NAFLD, compensatory mitochondrial adaptation is induced to counteract fat accumulation; at these stages, increased mitochondrial respiratory activity, biogenesis, and mass are observed [10,11]. However, compensatory metabolic responses are lost during NAFLD progression. Although higher mitochondrial biogenesis and mass are observed at these stages, it is characterized by lower respiration rates, an imbalance of mitochondrial dynamics, and increased oxidative stress [12–14]. This indicates that the degradation of damaged mitochondria is defective, resulting in a lower density of functional mitochondria [13]. Therefore, the maintenance of mitochondrial dynamics and function is crucial for hepatic lipid metabolism and integrity.

Copines (CPNE) are a Ca^{2+}-dependent phospholipid-binding protein family that has two C2 domains (C2A and C2B) and one von Willebrand factor A domain [15]. The C2 domain is involved in Ca^{2+}-dependent phospholipid binding, and the von Willebrand factor A domain is known to mediate protein-protein interactions by binding to the tetratricopeptide repeat domain [16]. Copines exist ubiquitously in most eukaryotes, except yeast and Drosophila, and are generally present as a family of multiple homologs [15]. The high degree of conservation and multiplicity of this copine family suggests that copines play a fundamental role in cell biology. Copines are involved in the development and differentiation of the nervous system as well as the occurrence and development of numerous tumor types. The immune microenvironment of tumors is affected by Copines [17]. Recent studies have consistently reported that the copine family is associated with the lipid metabolic pathway; the low expression of *CPNE3* is associated with the risk of acute myocardial infarction in patients with stable coronary artery disease and genetic variants of *CPNE5* were associated with obesity [18, 19]. Moreover, a study reported that whole-exome sequencing and genome-wide association analyses of Nunavik Inuit revealed a high frequency of *ICAM5, STAT2, RAF1*, and particularly *CPNE7* gene variants. These gene variants including *CPNE7* were associated abnormalities in fatty acid and lipid metabolism, increasing genetic risk responsible for a predisposition to metabolic syndrome [20].

Considering the findings of previous studies, it is indispensable to investigate the relationship between lipid metabolism and *Cpne7*. Therefore, this study aims to explore the role of *Cpne7* in the liver, which is the central organ of lipid metabolism based on mitochondrial function.

2. Methods

2.1. Animals

All animal procedures were approved by the Institutional Animal Care and Use Committee of Seoul National University (SNU-210208-4-1). This study also conformed to the ARRIVE guidelines and was performed in accordance with the National Research council's Guide for the Care and Use of Laboratory Animals. C57BL/6 mice were purchased from Dooyeol Biotech (Seoul, Korea), and the *Cpne7*-null (*Cpne7*$^{-/-}$) mice were created by deleting Exons 5, 6, and 7 of the *Cpne7* gene through the CRISPR/Cas9 system and cloning a vector containing EGFR and NeoR by Macrogen (Seoul, Korea). The cloned vector was transformed using the electroporation method in the CMTI-1 ES cell line derived from 129/SVEV mice. After electroporation, G418/ganciclovir-resistant colonies were selected and transplanted into surrogate mothers to generate offspring. *Cpne7*$^{-/-}$ mice were identified by PCR. The primers used were exon7 F (5′-CAGAAGGCCTTTGAGGAGGAGC-3′, deleted region), neo F (5′-CAA TATGGGATCGGCCATTGAAC -3′, *Cpne7*$^{-/-}$ vector sequence) and exon8 RR (5′-GTTTGTACTTGGCAT TCACACAGTCC-3′). The schematic diagram of generation of Cpne7 $^{-/-}$ mice is found in the Supplementary Fig. 1. Experiments were performed on male mice. All mice used in the experiment were housed in cages with a 12:12-h light/dark cycle at about 20° C-25 °C and 45%–55 % humidity.

2.2. RNA-sequencing analysis

Total RNA was extracted from homogenized liver tissues of 1-month-old wild-type (WT) and *Cpne7*$^{-/-}$ mice (n = 3) using the TRIzol reagent per the manufacturer's instructions (Invitrogen, Carlsbad, CA, USA). The total RNA (2 μg) of each group was shipped in a freezing container to Macrogen. RNA-seq library construction was performed using the TruSeq Stranded mRNA LT Sample Prep Kit (Illumina, San Diego, CA, USA). cDNA libraries were produced via the purification of total RNA, random fragmentation, and reverse transcription into cDNA. The libraries were sequenced using the NovaSeq 6000 system (Illumina). The detailed procedure is found in the supporting information.

For the list of significant differentially expressed genes, the Gene set enrichment analysis in a biological process and molecular function, was performed using gProfiler (https://biit.cs.ut.ee/gprofiler/orth). The functional protein association networks were conducted using String database (https://string-db.org).

2.3. HFD-induced NAFLD model

The control WT and *Cpne7*$^{-/-}$ mice (n = 6) were fed a chow diet (CD; 2018s, Envigo, Udine, Italy). For NAFLD induction, the experimental WT and *Cpne7*$^{-/-}$ mice (n = 6) were fed a 60 % high-fat diet (HFD; TD.06414, Envigo). The diet composition is found in

the supporting information. The HFD was performed on 6-week-old male mice for 16 weeks. At each HFD replacement, residual feeds were monitored to ensure that food consumption was not affecting the results. After CD or HFD feeding for 16 weeks, the mice were anesthetized with a 2.5 % 2-methyl-2-butanol (Avertin; 240,486, Sigma-Aldrich, MO, USA) solution diluted with RNase-free water (BWA-8000, T&I, Korea). Subsequently, the body and liver weights were measured, and a macroscopic analysis of the body and liver was conducted.

2.4. Serum analysis

The mice (n = 4) were anesthetized, and blood samples were collected via cardiac puncture after overnight fasting prior to their sacrifice. The whole blood was centrifuged at 2000 g for 10 min to obtain serum. The obtained serum was shipped in freezing containers to GCCL (Yongin, Korea). The serum levels of albumin (g/dL), alanine aminotransferase (ALT; U/L), total cholesterol (T. col; mg/dL), triglyceride (TG; mg/dL), free fatty acid (FFA; μEq/L), and glucose (mg/dL) were measured through GCCL.

2.5. Hematoxylin and eosin (H&E) staining

The harvested tissues (n = 6) were fixed in 4 % paraformaldehyde in PBS at 4 °C for a day. Subsequently, dehydration, clearing, and paraffin infiltration were performed using an automatic tissue processor (TP 1020, Leica, Wetzlar, Germany). The tissues were embedded in paraffin and sectioned into 5-μm-thick slices using a microtome (RM 2155, Leica, Wetzlar, Germany). After deparaffinization and rehydration, these sections were stained with H&E, dehydrated, cleared, and mounted.

For lipid droplet (LD) quantification, the void area occupied by lipid infiltrates in the H&E-stained images at × 400 was analyzed using the particle analysis of Image J (National Institute of Health, USA). To exclude central veins and liver sinusoids, the size of the measurement range was set to 20–5000 μm^2, and the circularity was set to 0.5–1.0. The percentage of steatosis is the ratio of area covered by lipids to total area.

2.6. Transmission electron microscopy (TEM) analysis

The harvested tissues were fixed in Karnovsky's fixative at 4 °C for 4 h. Subsequently, the tissues were post-fixed in 1 % osmium tetroxide diluted in 0.1-M sodium cacodylate buffer. After *en bloc* staining with 0.5 % uranyl acetate, dehydration was performed using a graded ethanol series and propylene oxide, and the infiltration of Spurr's resin was conducted. The polymerized blocks were sectioned using an ultramicrotome (Leica, EM UC6). TEM images were obtained using JEM-1400 Flash.

2.7. Cell culture and transfection

The HepG2 cell line was purchased from the Korea Cell Line Bank (Seoul, Korea, KCLB no.88065). HepG2 cells were grown and maintained in MEM (Gibco BRL, Carlsbad, CA, USA) supplemented with 10 % FBS (Gibco BRL) and antibiotic-antimycotic reagents (Gibco BRL) at 37 °C in a humidified 5 % CO_2 atmosphere.

The expression vector encoding DDK (Flag)-tagged *CPNE7* (NM_153,636) was purchased from Origene (Rockville, MD, USA). Control shRNA (sc-37007) and *CPNE7* shRNA (sc-93065-SH) were purchased from Santa Cruz Biotechnology. The HepG2 cells were seeded in 60 mm culture dishes at a density of 5×10^5 cells per well. The cells were transfected with DDK (Flag)-tagged *CPNE7* and sh*CPNE7* using the Metafectene Pro reagent (Biontex, Marinsried, Germany) per the manufacturer's instructions.

2.8. Western blot

Western blotting was performed as previously described [21]. Liver tissue samples were homogenized using ice-cold RIPA buffer with a homogenizer (SuperFastPrep-2, #6012500, MP Biomedicals, USA). The cells were lysed using ice-cold RIPA buffer. The liver homogenates and lysed cells were centrifuged at 13,000 rpm for 30 min, and the supernatant was collected. Proteins (5–40 μg) were loaded into the polyacrylamide gel and probed primary antibody. Antibodies used are listed in the supporting information. *Anti*-CPNE7 were produced as previously described [22]. After incubation with the secondary antibody, protein loading was measured by the expression of GAPDH. Semi-quantitative assessments were conducted using Image Studio Lite (Version 5.2, Li-cor, Lincoln, NE, USA).

2.9. Measurement of ROS levels

ROS levels were analyzed using a ROS assay kit (ab113851, Abcam, Cambridge, UK). The ROS assay was performed per the manufacturer's instructions. Deparaffinized tissue sections were incubated with the 2, 7-Dichlorofluorescin diacetate (DCFDA) solution for 45 min at 37 °C in the dark. After being washed, the tissue sections were stained with 4′, 6-diamidino-2-phenylindole (DAPI) for 5 min. Subsequently, the mounting procedure (s3023, DAKO, Copenhagen, Denmark) was conducted. ROS levels of tissue sections were measured via confocal laser scanning microscopy (CarlZeiss, LSM 800) at Ex/Em = 485/535 nm.

The cells were seeded 96-well microplates with 25,000 cells per well. After incubation overnight, the cells were stained by adding the DCFDA solution for 45 min at 37 °C in the dark. Subsequently, the DCFDA solution was removed and H_2O_2 (1 mM) was treated for 4 h. The plates were measured on a fluorescence plate reader at Ex/Em = 485/535 nm.

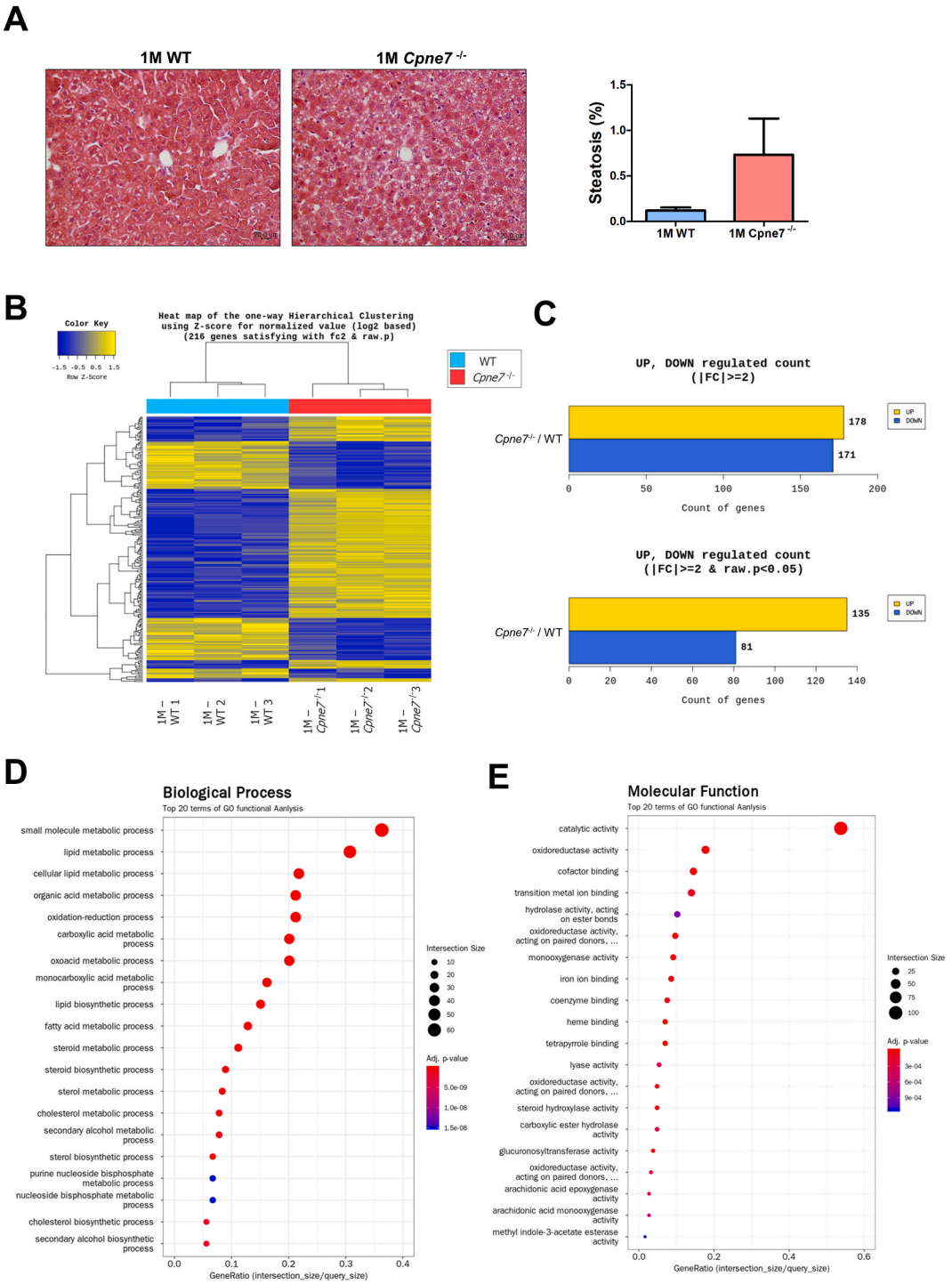

Fig. 1. Numerous lipid droplets and differentially expressed genes are observed in the livers of chow diet (CD)-fed *Cpne7*-null (*Cpne7*$^{-/-}$) mice. (A) H&E-stained images in the livers of 1-month-old wild-type (WT) and *Cpne7*$^{-/-}$ mice (scale bars = 20 μm). (B–F) RNA-sequencing analysis on liver homogenates. (B) Heat map for hierarchical clustering. The left column represents WT control, and the right column represents *Cpne7*$^{-/-}$ group. Each row represents a single gene. The color change from yellow to blue lg (FPKM+1) value ranging from high to low. (C) The number of differentially expressed genes by fold change (n = 3). (D, E) GO functional analysis. (For interpretation of the references to color in this figure legend, the reader is referred to the Web version of this article.)

2.10. Measurement of mitochondrial function

Oxygen consumption rate (OCR) was measured by Seahorse XFe96 Extracellular Flux Analyzer with XF Cell Mito Stress Test Kit as per manufacturer's protocol (Seahorse Bioscience, North Billerica, MA, USA). Briefly, HepG2 cells were treated using H_2O_2 (200 μM, 24h) following transfection of control, sh*CPNE7* and *CPNE7* o/e and were seeded at a density of 2×10^4 cells/well onto 96-well cell culture plate for overnight. The medium was replaced the following day to XF running medium with 2 mM L-glutamine and 1000 mg/L D-glucose for OCR measurement. Cells were sequentially exposed to Oligomycin (1.5 μM; ATPase inhibitor), FCCP (0.5 μM; mitochondrial uncoupler) and Rotenenone/Antimycin A (0.5 μM; complex I/III inhibitor). The average measurement from experiments conducted in triplicate is shown by each point in the traces.

2.11. Oil-red O staining

After treatment with H_2O_2 (200 μm) for 24 h, HepG2 cells were fixed in 10 % formalin (Junsei Chemical, Japan) for 30 min. After being washed, the cells were incubated in 60 % isopropanol (Duksan, Korea) for 5 min and covered in the oil-red O solution (Sigma-Aldrich) for 20 min. After being washed, the cells were counterstained using hematoxylin for 1 min and washed with distilled water, followed by viewing under a microscope. For quantification, after staining with hematoxylin and washing, the cells were washed using 60 % and 100 % isopropanol, and then the supernatant was used to read the absorbance at 492 nm.

2.12. Statistical analysis

Statistical analyses were performed using GraphPad Prism software (version 5, GraphPad Software, CA, USA). All values are expressed as the mean ± standard deviation for at least three independent experiments. Between-group statistical analyses were performed using the independent *t*-test or one-way analysis of variance followed by Tukey's post-hoc test. Statistically significant differences between groups were considered at $^*p < 0.05$, $^{**}p < 0.01$ and $^{***}p < 0.001$.

3. Results

3.1. Cpne7 deficiency is associated with impaired hepatic lipid metabolism under normal conditions

3.1.1. Hepatic fatty changes occur in CD-fed Cpne7 $^{-/-}$ mice

To investigate whether *Cpne7* is involved in hepatic lipid metabolism, histological analysis was conducted in the livers of WT and *Cpne7*$^{-/-}$ mice. In the H&E-stained images, several LDs were observed in the livers of *Cpne7*$^{-/-}$ mice compared with WT mice, although there was no statistical difference (Fig. 1A). This result suggests that *Cpne7* is linked to hepatic lipid metabolism.

3.1.2. Cpne7 deficiency is involved in dysregulated lipid metabolism and mitochondrial dysfunction in RNA-sequencing analysis of liver tissues

To determine the difference in lipid metabolism-related gene expression, RNA-sequencing was performed in liver tissues of WT and *Cpne7*$^{-/-}$ mice (n = 3). As a result of RNA-sequencing, the significant gene expression pattern, as seen through the heat map, was different in the livers of WT and *Cpne7*$^{-/-}$ mice (Fig. 1B). There were 178 upregulated genes and 171 downregulated genes in the livers of *Cpne7*$^{-/-}$ mice compared with those of WT mice on the condition of $|\text{fold change (FC)}| \geq 2$. Among the genes, 135 genes were significantly increased, and 81 genes were significantly decreased in the livers of *Cpne7*$^{-/-}$ mice compared with those of WT mice (Fig. 1C).

Subsequently, a Gene Ontology (GO) enrichment analysis targeting the list of significant differentially expressed genes was performed. The top 20 GO terms satisfying the p-value <0.05 for each category were presented as a dot plot. Most GO terms in the biological process were associated with lipid metabolism processes such as the lipid metabolic, lipid biosynthetic, fatty acid metabolic, and cholesterol metabolic processes (Fig. 1D). The top GO terms in molecular functions were catalytic activity and oxidoreductase activity related to mitochondrial functions (Fig. 1E).

The functional protein association networks were conducted using the list of significant differentially expressed genes (Supplementary Fig. 2). The line represents protein-protein associations. Each node (circles) represents all the proteins produced by a single, protein-coding gene locus. The node color indicates the corresponding GO terms. The interaction network showed that genes involved in lipid metabolism, fatty acid metabolism, insulin receptor signaling, and antioxidant activity were organically linked.

As can be seen in the list of significant differentially expressed genes related of lipid metabolism of Supplementary Table 1, sterol regulatory element binding transcription factor 1 (*Srebf1*), a transcription factor for lipogenesis, and downstream lipogenic genes were upregulated in the livers of *Cpne7*$^{-/-}$ mice compared with those of WT mice. Furthermore, fatty acid synthesis genes such as *Acot1, Acot11, Fabp2, Gpcpd1, Nudt7, Pex11a, Pex11a and Plcg1* were upregulated in the livers of *Cpne7*$^{-/-}$ mice compared with those of WT mice. Conversely, the leptin receptor (*Lepr*) and insulin-like growth factor-binding protein 1 (*lgfbp1*) were downregulated in the livers of *Cpne7*$^{-/-}$ mice compared with those of WT mice.

In the list of significant differentially expressed genes related of oxidoreductase activity, the expression of cytochrome P450 (Cyps) family, which is mostly found in the mitochondria and endoplasmic reticulum (ER), was altered. Additionally, NADPH oxidase 4 (*Nox4*), which causes oxidative stress, was upregulated and the genes with antioxidant activity such as *Mgst3, Nqo1, and S100a9* were downregulated in the livers of *Cpne7*$^{-/-}$ mice compared with those of WT mice (Supplementary Table 1). These results indicate the

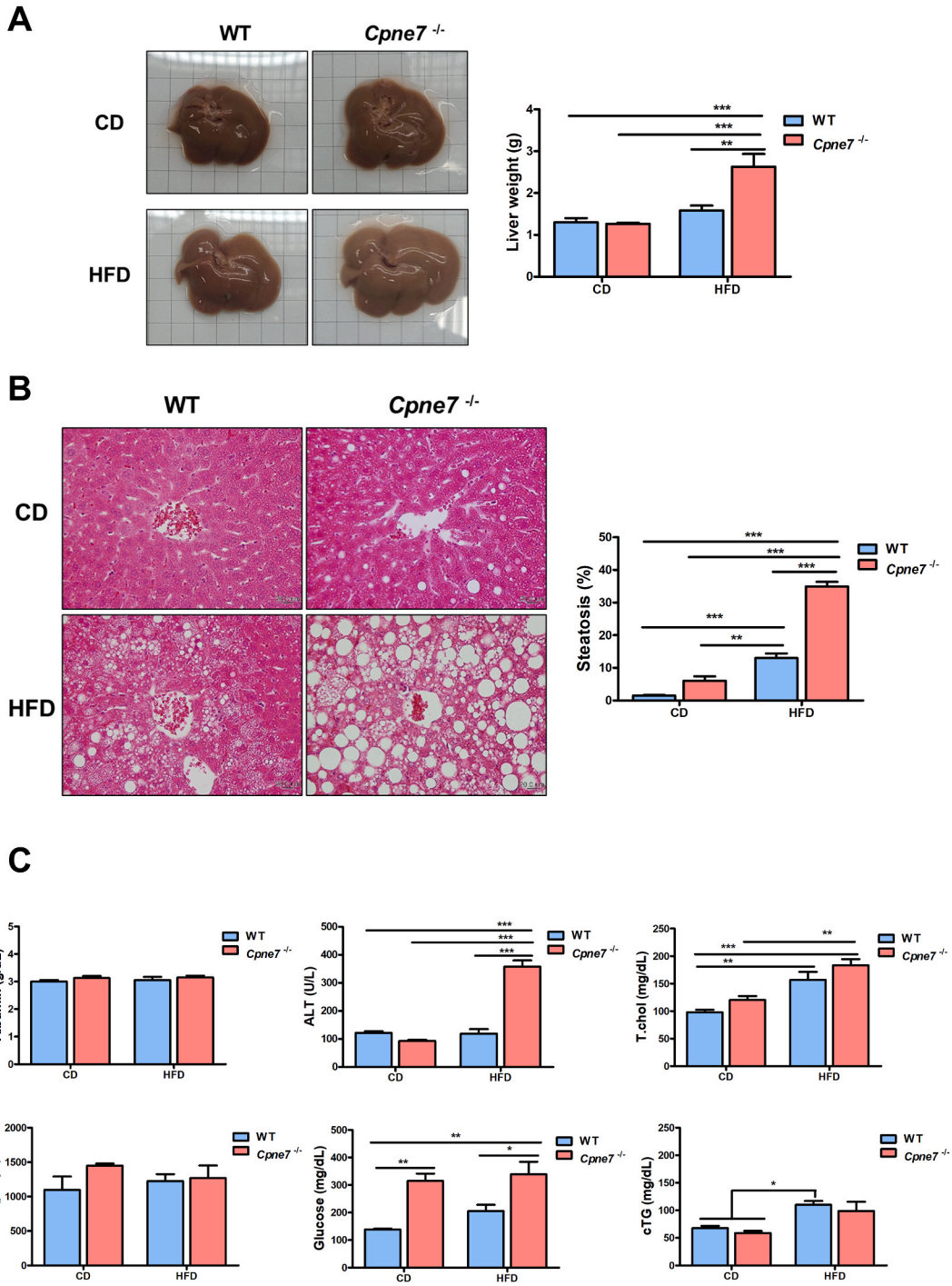

Fig. 2. *Cpne7* deficiency accelerates hepatic fatty changes in the HFD-induced NAFLD model. (A) Representative macroscopic liver images and liver weights in CD-fed and HFD-fed WT and *Cpne7*$^{-/-}$ mice. (B) H&E-stained images in the livers of CD-fed and HFD-fed WT and *Cpne7*$^{-/-}$ mice (scale bars = 20 μm), and quantitative analysis of percentage of steatosis using Image J software. (C) Serum levels of albumin, alanine aminotransferase (ALT), total cholesterol (T.chol), triglyceride (TG), free fatty acid (FFA), and glucose in CD-fed and HFD-fed WT and *Cpne7*$^{-/-}$ mice. (*$p < 0.05$, **$p < 0.01$ and ***$p < 0.001$).

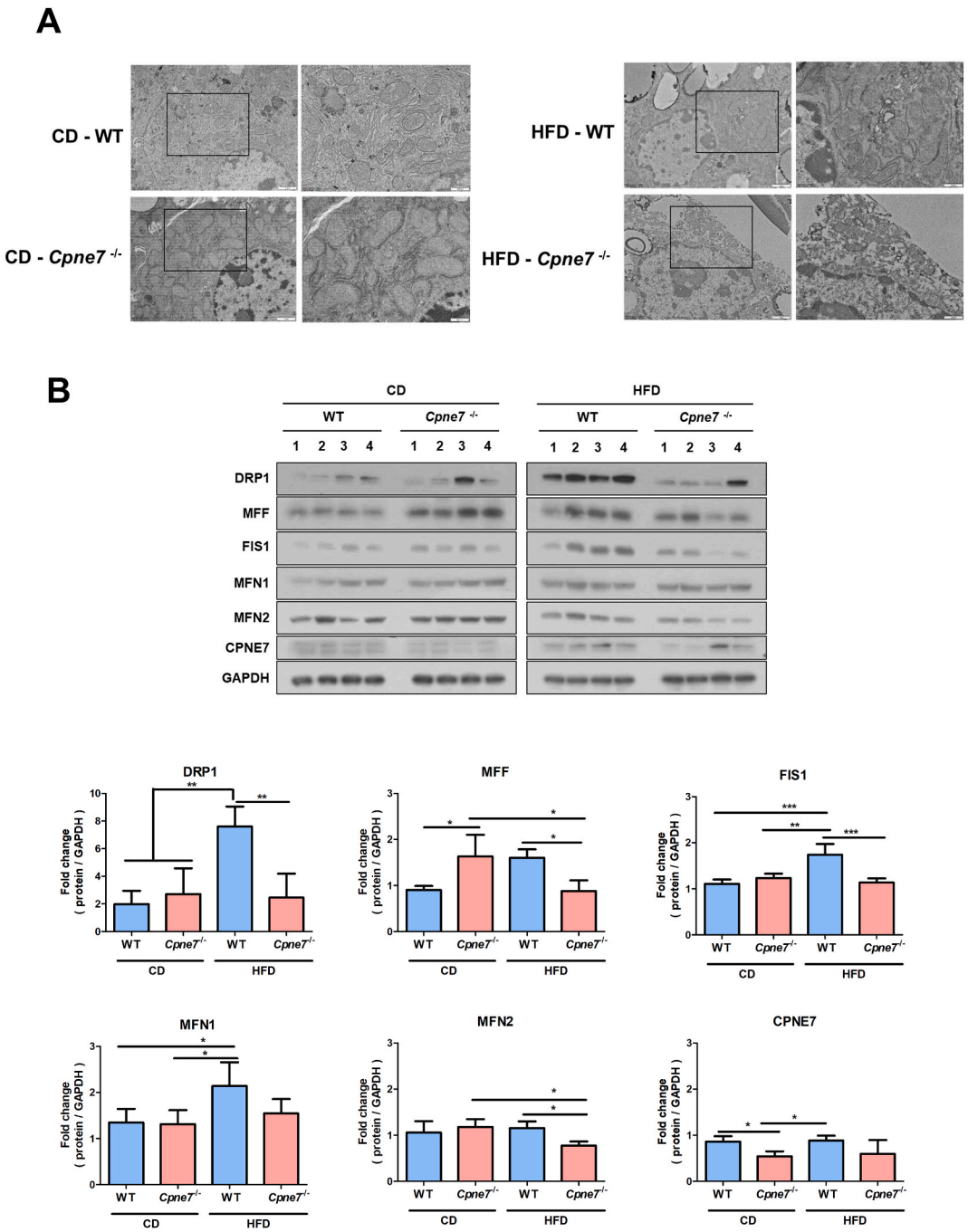

Fig. 3. *Cpne7* deficiency induces abnormal mitochondrial dynamics and excessive ROS production *in vivo*. (A) TEM images in the livers of CD-fed and HFD-fed WT and *Cpne7*$^{-/-}$ mice. The right column (scale bars = 1 μm) was investigated under magnification of the left column (boxed area, scale bars = 500 nm). (B) Western blot analysis of mitochondrial fission and fusion protein levels in the livers of CD-fed and HFD-fed WT, *Cpne7*$^{-/-}$ and *Cpne7* Tg mice, and quantification of mitochondrial fission and fusion protein levels. The uncropped version is available in the supplementary file. (C) Representative fluorescence images of DCFDA for ROS detection in the livers of CD-fed and HFD-fed WT and *Cpne7*$^{-/-}$ mice. Images were used of pseudo-color look-up table (LUT). The LUT setting were assigned for pixels with blue of low intensity, yellow of intermediate intensity and red of high intensity (scale bars = 50 μm) and quantification of ROS levels. (*$p < 0.05$, **$p < 0.01$ and ***$p < 0.001$). (For interpretation of the references to color in this figure legend, the reader is referred to the Web version of this article.)

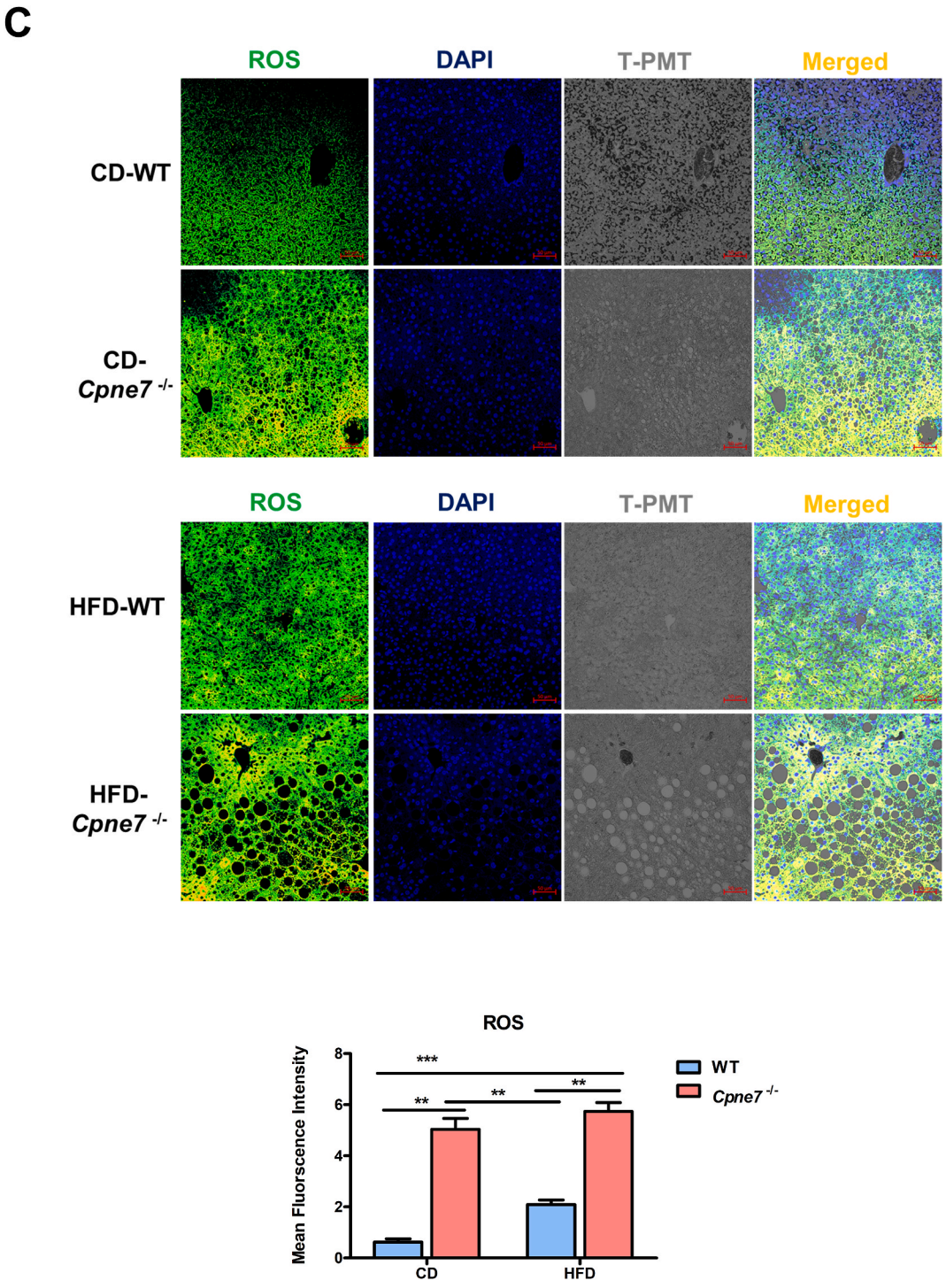

Fig. 3. (*continued*).

possibility that *Cpne7* deficiency could affect hepatic lipid metabolism and mitochondrial function.

3.2. Cpne7 deficiency destroys lipid metabolism and mitochondrial redox balance in the HFD-induced NAFLD model

3.2.1. Cpne7 deficiency exacerbates hepatic steatosis in the HFD-induced NAFLD model

To examine the effect of *Cpne7* on the hepatic lipid metabolism, we established a HFD-induced NAFLD model. HFD feeding was

performed in WT and *Cpne7*$^{-/-}$ mice for 16 weeks (n = 6). In the HFD-induced NAFLD model, macroscopic analyses demonstrated that the livers of *Cpne7*$^{-/-}$ mice were larger and had more pale-yellow appearances than those of WT mice. Moreover, liver weights of HFD-fed mice were significantly increased in *Cpne7*$^{-/-}$ mice compared to WT mice (Fig. 2A).

During histological analyses, several LDs were observed in the livers of *Cpne7*$^{-/-}$ mice even among CD-fed mice. The livers of HFD-fed *Cpne7*$^{-/-}$ mice showed severe steatosis features such as excessive lipid accumulation and hepatocyte ballooning. According to LD quantification in the H&E-stained images, in HFD-fed mice, the percentage of steatosis were significantly higher in *Cpne7*$^{-/-}$ mice than in WT mice (Fig. 2B).

Additionally, blood tests in each group were performed after overnight fasting. Regarding the levels of liver damage markers, the ALT levels of HFD-fed *Cpne7*$^{-/-}$ mice were significantly increased compared to those of WT mice. Furthermore, glucose levels were significantly increased in CD- and HFD-fed *Cpne7*$^{-/-}$ mice compared to WT mice (Fig. 2C). Investigation of the effect on whole-body lipid metabolism revealed that there was no significant difference in body weight, but a significant increase in fat percentage in HFD-fed *Cpne7*$^{-/-}$ mice compared to HFD-fed WT mice (Supplementary Fig. 3). These results suggest that *Cpne7* deficiency accelerates hepatic lipid accumulation in the HFD-induced NAFLD model, resulting in hepatotoxicity and abnormal lipid metabolism.

3.2.2. *Cpne7* deficiency leads to mitochondrial dysfunction and elevated ROS levels in the livers in vivo

To identify how *Cpne7* deficiency induced lipid accumulation, we analyzed mitochondrial function, which is known to be strongly associated with lipid metabolism [10,23–25]. A TEM analysis was performed to compare the mitochondrial morphology. In CD-fed mice, the hepatic mitochondria of *Cpne7*$^{-/-}$ mice were swollen and lost cristae; however, those of WT mice did not. The hepatic mitochondria of HFD-fed WT mice were swollen, and cristae loss was observed compared to those of CD-fed WT mice. The most striking result to emerge from TEM data is that most of the mitochondria were damaged, and abnormal mitochondrial morphologies were observed due to severe cell injury in the livers of HFD-fed *Cpne7*$^{-/-}$ mice (Fig. 3A). In the marker expression analysis of mitochondrial dynamics, both fission regulators such as DRP1, MFF, and FIS1 and fusion regulators such as MFN1 and MFN2 were

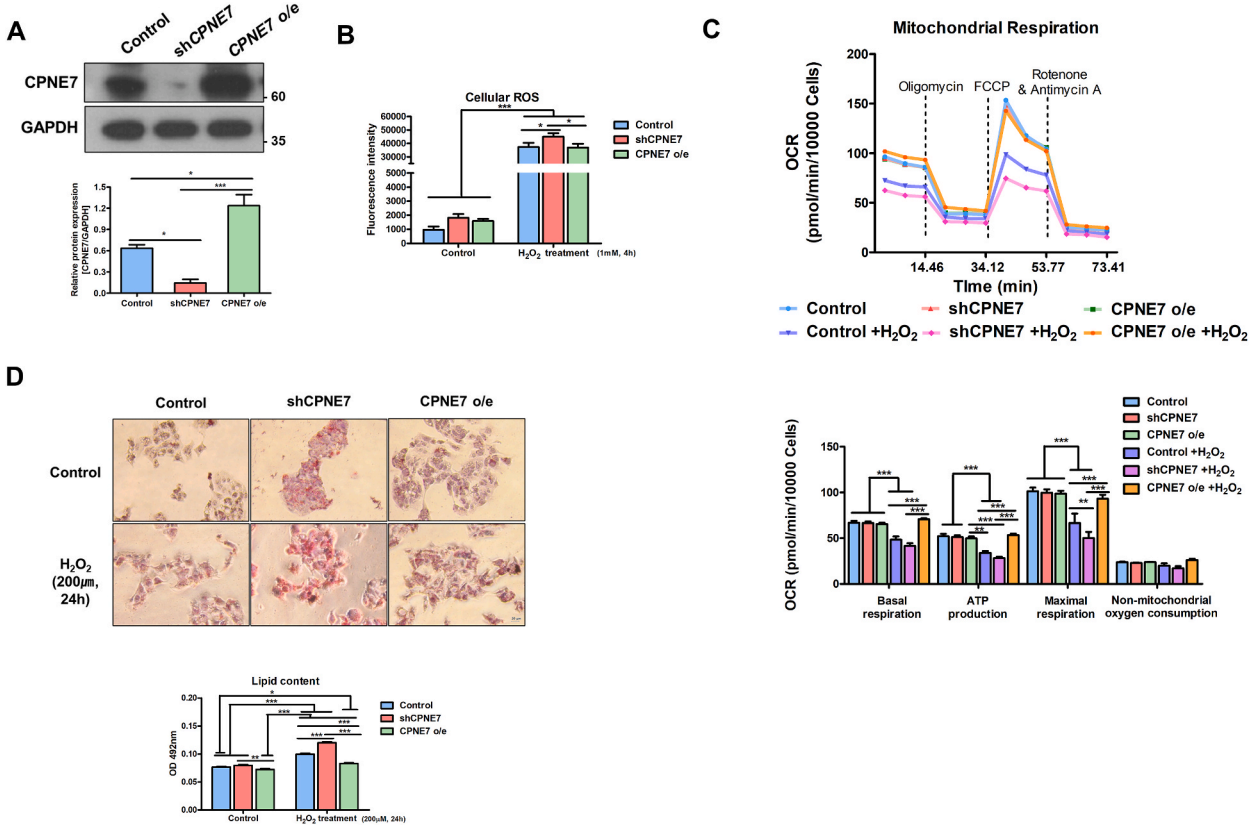

Fig. 4. *CPNE7* overexpression rescues *CPNE7* silencing-induced mitochondrial dysfunction and lipid accumulation in H_2O_2-damaged HepG2 cells. (A) CPNE7 expression by western blotting to assess the efficiency of sh*CPNE7*, and *CPNE7* overexpression vector (o/e) transfection in HepG2 cells. The uncropped version is available in the supplementary file. (B) Fluorescence intensity of cellular ROS in control, sh*CPNE7*, and *CPNE7* o/e transfected HepG2 cells with control and H_2O_2-induced oxidative stress. (C) Representative and statistical results of mitochondrial respiration in control, shCPNE7, and CPNE7 o/e transfected HepG2 cells with control and H_2O_2-induced oxidative stress (D) Oil-red O staining for detection of lipid content in control, sh*CPNE7*, and *CPNE7* o/e transfected HepG2 cells with control and H_2O_2-induced oxidative stress (scale bars = 20 μm) and quantification of oil-red O analysis. (*p < 0.05, **p < 0.01 and ***p < 0.001). (For interpretation of the references to color in this figure legend, the reader is referred to the Web version of this article.)

significantly decreased in the livers of HFD-fed *Cpne7*$^{-/-}$ mice compared to those of HFD-fed WT mice (Fig. 3B). Furthermore, the RNA levels of mitochondrial oxidative phosphorylation subunits (CI- CV) are downregulated in the livers of HFD-fed *Cpne7*$^{-/-}$ mice (Supplementary Fig. 4). To assess whether *Cpne7* deficiency could elicit excessive ROS production, we measured the ROS levels. High ROS production was observed in the livers of CD-fed and HFD-fed *Cpne7*$^{-/-}$ mice (Fig. 3C). These findings suggest that *Cpne7* deficiency results in excessive ROS formation as well as hepatic mitochondrial damages such as abnormal morphology and decreased mitochondrial dynamics.

3.3. CPNE7 overexpression restores hepatic mitochondrial dysfunction and lipid accumulation caused by CPNE7 silencing under oxidative stress in vitro

To validate the role of *CPNE7* in hepatocytes *in vitro*, HepG2 cells were transfected with shRNA and expression vectors of *CPNE7*. The transfection efficiency was evaluated via protein levels of CPNE7. Compared with controls, protein levels of CPNE7 were significantly decreased and increased by sh*CPNE7* and *CPNE7* overexpression (o/e), respectively (Fig. 4A). Cellular ROS in H_2O_2-treated HepG2 cells was significantly increased compared to HepG2 cells not treated with H_2O_2. In H_2O_2-induced oxidative stress, cellular ROS was increased in *CPNE7*-silenced cells compared with controls, and *CPNE7*-overexpressed cells showed decreased ROS levels compared with *CPNE7*-silenced cells (Fig. 4B). Mitochondrial respiration in H_2O_2-treated HepG2 cells was significantly decreased compared to HepG2 cells not treated with H_2O_2. In H_2O_2-induced oxidative stress, maximal respiration is significantly reduced in *CPNE7*-silenced cells compared with controls, *CPNE7*-overexpressed cells showed increased mitochondrial function including basal respiration, ATP production, and maximal respiration (Fig. 4C). In the results of oil-red O staining, lipid contents in H_2O_2-treated HepG2 cells were significantly increased compared to HepG2 cells not treated with H_2O_2. *CPNE7*-silenced cells showed markedly increased lipid contents, and lipid contents in *CPNE7*-overexpressed cells were significantly decreased compared with those of controls under H_2O_2-induced oxidative stress (Fig. 4D). These results implicate that *CPNE7* silencing promotes hepatic lipid accumulation by causing excessive ROS production and mitochondrial dysfunction under H_2O_2-induced oxidative stress, whereas *CPNE7* overexpression returns mitochondrial function and lipid metabolism to normal conditions.

4. Discussion

Previous studies have emphasized that hepatic mitochondria play a role in the pathogenesis of NAFLD [3,26,27]. In this study, we investigated whether *Cpne7* affects hepatic lipid metabolism and mitochondrial function using *Cpne7*$^{-/-}$ mice *in vivo* and *Cpne7*-silenced and *Cpne7*-overexpressed HepG2 cells *in vitro*. The differentially expressed genes in the livers of *Cpne7*$^{-/-}$ mice were involved in lipogenesis and mitochondrial dysfunction. *Srebf1*, a transcription factor for lipogenesis [28], was increased, and most of its downstream lipogenic genes were significantly increased. Fatty acid synthesis genes were significantly upregulated. In addition, hormone-related genes, such as *Lepr* and *Igfbp1*, were downregulated, linking that not only fat accumulation but also insulin resistance [29,30]. In differentially expressed genes with oxidoreductase activity, changes in the *Cyps* expression were noticeable. Considering that *Cyps* are expressed in mitochondria and plays roles in xenobiotics and steroid hormone metabolism [31–33], changes of these gene expression could be related to mitochondrial function, hepatotoxicity, and insulin resistance. Furthermore, *Cyps* and *Nox4* are known the sources of ROS [34,35]. In contrast, there was a downregulation of genes involved in antioxidant activity such as *Mgst3*, *Nqo1*, and *S100a9*. Similar alterations in these gene expression levels occurred in the livers of CD- and HFD-fed *Cpne7*$^{-/-}$ mice (Supplementary Fig. 5). These findings suggest that *Cpne7* deficiency could cause lipogenesis, elevated ROS levels, and mitochondrial dysfunction.

Typical pathological manifestations of NAFLD, such as increased liver sizes, pale-yellow appearances, severe steatosis, and hepatocyte ballooning, were accelerated in the livers of HFD-fed *Cpne7*$^{-/-}$ mice compared with those of HFD-fed WT mice. Additionally, numerous LDs were observed in the livers of CD-fed *Cpne7*$^{-/-}$ mice but not in those of CD-fed WT mice. Interestingly, *Cpne7* deficiency not only resulted in fatty changes in the liver but also mitochondrial dysfunction. Abnormal mitochondrial morphology and high ROS levels were observed in CD-fed and HFD-fed *Cpne7*$^{-/-}$ mice. Furthermore, in line with the results of *in vivo* investigations, high ROS levels, mitochondrial dysfunction and lipid accumulation were observed in H_2O_2-damaged sh*CPNE7* HepG2 cells.

These results align with several previous studies indicating that mitochondrial ultrastructural abnormalities appeared with increasing NAFLD severity [36–39]. The deterioration of the mitochondrial morphology may indicate an increase in oxidative stress and the disruption of the biological system regulating mitochondrial biogenesis, mitophagy, fission and fusion [25]. Mitochondria are dynamic organelles in which fission and fusion occur continuously. Mitochondrial dynamics are involved in the quality control mechanism that maintains mitochondrial function [40,41]. Mitochondrial morphology can be modulated by the structural components and signaling pathways [41]. Changes in mitochondrial morphology help mitochondria adapt to specific cellular and tissue demands and regulates mitochondrial reaction to cytosolic signals [42]. Therefore, mitochondrial fusion and fission are key events regulating normal mitochondrial function and prevent disease [43]. Mitochondrial fusion is mediated by two mitofusins (MFN1 and MFN2) and optic atrophy1 (OPA1). MFN1 fuse the inner mitochondrial membrane (IMM) with OPA1 and the outer mitochondrial membrane (OMM) with MFN2 [44,45]. In addition, MFN2 participate in tethering mitochondrion to mitochondrion and mitochondria to other organelles [46,47]. Mitochondrial fission is primarily regulated by dynamin-related protein 1 (DRP1), mitochondrial fission factor (MFF) and mitochondrial fission 1 protein (FIS1). DRP1 oligomerizes and drive fragmentation [48]. FIS1 and MFF functions as a DRP1 receptors to recruit DRP1 [49,50].

Several reports have shown that DRP1, a key regulator of mitochondrial fission, was reduced in a rodent model of western diet-induced NASH and liver-specific deletion of DRP1 caused the loss of fatty acid oxidation [51,52]. Consistent with the findings of previous studies, mitochondrial fission regulators such as DRP1, MFF, and FIS1 in the livers of HFD-fed *Cpne7*$^{-/-}$ mice were

significantly reduced compared to those of HFD-fed WT mice. This inhibition of mitochondrial fission could induce the accumulation of damaged mitochondria, which could exacerbate mitochondrial dysfunction [53,54]. Recently, Mary P. Moore et al. reported that the levels of markers of mitochondrial turnover decreased with the severity of human NAFLD and that low levels of these markers could trigger mitochondrial dysfunction and progression to NASH [25]. Based on the findings of these studies, we suggest that *Cpne7* deficiency causes mitochondrial dysfunction, exacerbating hepatic lipid metabolism.

However, there are some unanswered questions. In injury models such as HFD-fed *Cpne7*$^{-/-}$ mice or H_2O_2-treated sh*CPNE7* HepG2 cells, lipogenesis was noticeably increased, and mitochondrial function was significantly reduced. A similar pattern was also seen in the brain; *Cpne7*-knockout (KO) increased the amount of REM sleep in cage-changing or water immersion and restraint stress (WIPS) environments, whereas normal sleep was observed under basal conditions [55]. Therefore, the actions of CPNE7 appear to be more noticeable in response to environmental stimuli or stressful environments than in the basal condition. Although the mechanism is still unclear, it is speculated that CPNE7 is related to the homeostatic effect and further research is required. Additionally, further measurements of hepatic cholesterol and TG levels are needed since neither serum cholesterol nor cTG levels in HFD-fed *Cpne7*$^{-/-}$ mice were significantly elevated. HFD feeding in this study performed on young mice (6-week-old). Considering that metabolic diseases are closely involved in aging, further studies on the effect of *Cpne7* are needed in HFD-fed old mice (18-month-old). Furthermore, cellular-level assessment of mitochondrial morphology is required for determining mitochondrial abnormalities.

In summary, *Cpne7* deficiency in stressful environments causes mitochondrial dysfunction including imbalanced mitochondrial dynamics and reduced mitochondrial respiration, as well as excessive ROS formation. These abnormal biological processes lead to hepatic steatosis through upregulation of lipogenic genes and dysregulated fatty acid oxidation [14,26,56]. Conversely, excessive lipid accumulation has been reported to increase the formation of ROS [57,58]. The vicious cycle between the ROS formation, mitochondrial dysfunction, and lipogenesis aggravates the progression of NAFLD (Fig. 5). Therefore, this study shows that *Cpne7* deficiency deteriorates hepatic lipid metabolism by mitochondrial dysfunction and excessive ROS production. In contrast, CPNE7 overexpression can be alleviate aberrant lipid metabolism by modulating the mitochondrial function. In conclusion, this study highlights the critical role of *CPNE7* in hepatic mitochondrial function and the development of NAFLD, suggesting *Cpne7* as a novel therapeutic target for NAFLD. The insights gained from this study contribute to the understanding of the pathogenesis of NAFLD.

Funding

This work was supported by the Basic Science Research Program through the Ministry of Education of the Republic of Korea and National Research Foundation (NRF-2018R1A5A2024418) and the Bio & Medical Technology Development Program of the National

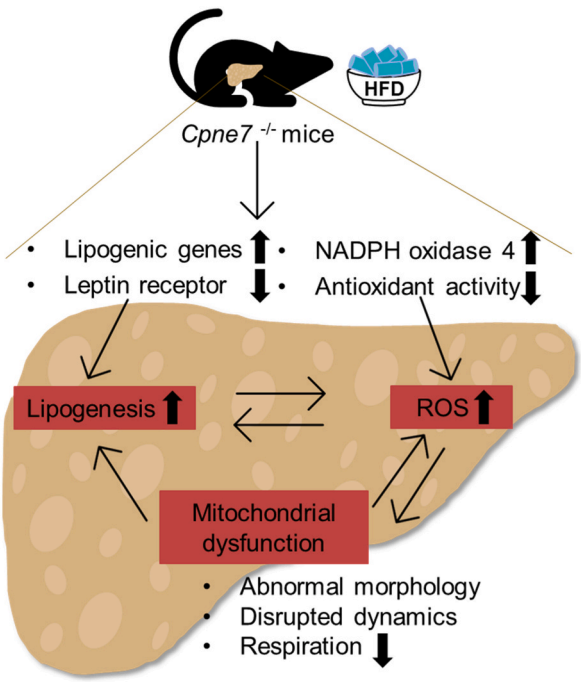

Fig. 5. Schematic illustration of effects of *Cpne7* on hepatocytes based on mitochondrial function. In the liver, *Cpne7* deficiency alters gene expression related to lipid metabolism and mitochondrial function. The differentially expressed genes lead to lipid droplet formation, high ROS levels, and dysregulated mitochondrial function in *Cpne7*$^{-/-}$ mice. Excessive ROS production causes mitochondrial dysfunction and lipogenesis, which in turns has a vicious cycle that induces high ROS levels. These pathological manifestations are exacerbated in an oxidative stress environment such as in the HFD-induced NAFLD model.

Research Foundation (NRF) & funded by the Korean government (MSIT) (No. 2022M3A9F3082330).

Ethics statement

All animal procedures were approved by the Institutional Animal Care and Use Committee of Seoul National University (SNU-210208-4-1). This study also conformed to the ARRIVE guidelines and was performed in accordance with the National Research council's Guide for the Care and Use of Laboratory Animals.

Data availability statement

The RNA-seq datasets presented in this study can be found in online repositories. The names of the repository/repositories and accession number(s) can be found below: SRA PRJNA879973, https://www.ncbi.nlm.nih.gov/sra/PRJNA879973.

CRediT authorship contribution statement

Geumbit Hwang: Writing – original draft, Visualization, Validation, Methodology, Investigation, Formal analysis, Conceptualization. **Hyejin Seo:** Methodology, Conceptualization. **Joo-Cheol Park:** Writing – review & editing, Supervision, Project administration, Funding acquisition.

Declaration of competing interest

The authors declare that they have no known competing financial interests or personal relationships that could have appeared to influence the work reported in this paper.

Acknowledgements

The authors thank PhD Yeoung-Hyun Park (HysensBio, Co., Ltd.) for providing technical support in the measurement of ROS levels by confocal laser scanning microscopy.

Appendix A. Supplementary data

Supplementary data to this article can be found online at https://doi.org/10.1016/j.heliyon.2023.e21676.

References

[1] D. Pessayre, A. Mansouri, D. Haouzi, B. Fromenty, Hepatotoxicity due to mitochondrial dysfunction, Cell Biol. Toxicol. 15 (1999) 367–373.
[2] J. Xu, J. Shen, R. Yuan, B. Jia, Y. Zhang, S. Wang, Y. Zhang, M. Liu, T. Wang, Mitochondrial targeting therapeutics: promising role of natural products in non-alcoholic fatty liver disease, Front. Pharmacol. 12 (2021), 796207.
[3] D. Pessayre, B. Fromenty, NASH: a mitochondrial disease, J. Hepatol. 42 (2005) 928–940.
[4] N.N. Than, P.N. Newsome, A concise review of non-alcoholic fatty liver disease, Atherosclerosis 239 (2015) 192–202.
[5] N. Chalasani, Z. Younossi, J.E. Lavine, A.M. Diehl, E.M. Brunt, K. Cusi, M. Charlton, A.J. Sanyal, The diagnosis and management of non-alcoholic fatty liver disease: practice Guideline by the American Association for the Study of Liver Diseases, American College of Gastroenterology, and the American Gastroenterological Association, Hepatology 55 (2012) 2005–2023.
[6] E. Bugianesi, S. Moscatiello, M.F. Ciaravella, G. Marchesini, Insulin resistance in nonalcoholic fatty liver disease, Curr. Pharmaceut. Des. 16 (2010) 1941–1951.
[7] I.A. Kirpich, L.S. Marsano, C.J. Mcclain, Gut-liver axis, nutrition, and non-alcoholic fatty liver disease, Clin. Biochem. 48 (2015) 923–930.
[8] A. Ferramosca, V. Zara, Modulation of hepatic steatosis by dietary fatty acids, World J. Gastroenterol. 20 (2014) 1746–1755.
[9] D. Degli Esposti, J. Hamelin, N. Bosselut, R. Saffroy, M. Sebagh, A. Pommier, C. Martel, A. Lemoine, Mitochondrial roles and cytoprotection in chronic liver injury, Biochem Res Int 2012 (2012), 387626.
[10] C. Koliaki, J. Szendroedi, K. Kaul, T. Jelenik, P. Nowotny, F. Jankowiak, C. Herder, M. Carstensen, M. Krausch, W.T. Knoefel, M. Schlensak, M. Roden, Adaptation of hepatic mitochondrial function in humans with non-alcoholic fatty liver is lost in steatohepatitis, Cell Metabol. 21 (2015) 739–746.
[11] E. Piccinin, G. Villani, A. Moschetta, Metabolic aspects in NAFLD, NASH and hepatocellular carcinoma: the role of PGC1 coactivators, Nat. Rev. Gastroenterol. Hepatol. 16 (2019) 160–174.
[12] M. Perez-Carreras, P. Del Hoyo, M.A. Martin, J.C. Rubio, A. Martin, G. Castellano, F. Colina, J. Arenas, J.A. Solis-Herruzo, Defective hepatic mitochondrial respiratory chain in patients with nonalcoholic steatohepatitis, Hepatology 38 (2003) 999–1007.
[13] L. Wang, X. Liu, J. Nie, J. Zhang, S.R. Kimball, H. Zhang, W.J. Zhang, L.S. Jefferson, Z. Cheng, Q. Ji, Y. Shi, ALCAT1 controls mitochondrial etiology of fatty liver diseases, linking defective mitophagy to steatosis, Hepatology 61 (2015) 486–496.
[14] A. Mansouri, C.H. Gattolliat, T. Asselah, Mitochondrial dysfunction and signaling in chronic liver diseases, Gastroenterology 155 (2018) 629–647.
[15] C.E. Creutz, J.L. Tomsig, S.L. Snyder, M.C. Gautier, F. Skouri, J. Beisson, J. Cohen, The copines, a novel class of C2 domain-containing, calcium-dependent, phospholipid-binding proteins conserved from Paramecium to humans, J. Biol. Chem. 273 (1998) 1393–1402.
[16] E.A. Nalefski, J.J. Falke, The C2 domain calcium-binding motif: structural and functional diversity, Protein Sci. 5 (1996) 2375–2390.
[17] H. Tang, P. Pang, Z. Qin, Z. Zhao, Q. Wu, S. Song, F. Li, The CPNE family and their role in cancers, Front. Genet. 12 (2021), 689097.
[18] K.S. Wang, L. Zuo, Y. Pan, C. Xie, X. Luo, Genetic variants in the CPNE5 gene are associated with alcohol dependence and obesity in Caucasian populations, J. Psychiatr. Res. 71 (2015) 1–7.
[19] B. Tan, L. Liu, Y. Yang, Q. Liu, L. Yang, F. Meng, Low CPNE3 expression is associated with risk of acute myocardial infarction: a feasible genetic marker of acute myocardial infarction in patients with stable coronary artery disease, Cardiol. J. 26 (2019) 186–193.

[20] S. Zhou, P. Xie, A. Quoibion, A. Ambalavanan, A. Dionne-Laporte, D. Spiegelman, C.V. Bourassa, L. Xiong, P.A. Dion, G.A. Rouleau, Genetic architecture and adaptations of Nunavik Inuit, Proc Natl Acad Sci U S A 116 (2019) 16012–16017.
[21] Y.M. Seo, S.J. Park, H.K. Lee, J.C. Park, Copine-7 binds to the cell surface receptor, nucleolin, and regulates ciliogenesis and Dspp expression during odontoblast differentiation, Sci. Rep. 7 (2017), 11283.
[22] J.H. Lee, D.S. Lee, H.W. Choung, W.J. Shon, B.M. Seo, E.H. Lee, J.Y. Cho, J.C. Park, Odontogenic differentiation of human dental pulp stem cells induced by preameloblast-derived factors, Biomaterials 32 (2011) 9696–9706.
[23] K.Y. Peng, M.J. Watt, S. Rensen, J.W. Greve, K. Huynh, K.S. Jayawardana, P.J. Meikle, R.C.R. Meex, Mitochondrial dysfunction-related lipid changes occur in nonalcoholic fatty liver disease progression, J. Lipid Res. 59 (2018) 1977–1986.
[24] A.P. Rolo, J.S. Teodoro, C.M. Palmeira, Role of oxidative stress in the pathogenesis of nonalcoholic steatohepatitis, Free Radic. Biol. Med. 52 (2012) 59–69.
[25] M.P. Moore, R.P. Cunningham, G.M. Meers, S.A. Johnson, A.A. Wheeler, R.R. Ganga, N.M. Spencer, J.B. Pitt, A. Diaz-Arias, A.I.A. Swi, G.M. Hammoud, J. A. Ibdah, E.J. Parks, R.S. Rector, Compromised hepatic mitochondrial fatty acid oxidation and reduced markers of mitochondrial turnover in human NAFLD, Hepatology (2022).
[26] K. Begriche, A. Igoudjil, D. Pessayre, B. Fromenty, Mitochondrial dysfunction in NASH: causes, consequences and possible means to prevent it, Mitochondrion 6 (2006) 1–28.
[27] D. Pessayre, A. Mansouri, B. Fromenty, Nonalcoholic steatosis and steatohepatitis. V. Mitochondrial dysfunction in steatohepatitis, Am. J. Physiol. Gastrointest. Liver Physiol. 282 (2002) G193–G199.
[28] J.D. Horton, J.L. Goldstein, M.S. Brown, SREBPs: activators of the complete program of cholesterol and fatty acid synthesis in the liver, J. Clin. Invest. 109 (2002) 1125–1131.
[29] O. Mammes, R. Aubert, D. Betoulle, F. Pean, B. Herbeth, S. Visvikis, G. Siest, F. Fumeron, LEPR gene polymorphisms: associations with overweight, fat mass and response to diet in women, Eur. J. Clin. Invest. 31 (2001) 398–404.
[30] A. Rajwani, V. Ezzat, J. Smith, N.Y. Yuldasheva, E.R. Duncan, M. Gage, R.M. Cubbon, M.B. Kahn, H. Imrie, A. Abbas, H. Viswambharan, A. Aziz, P. Sukumar, A. Vidal-Puig, J.K. Sethi, S. Xuan, A.M. Shah, P.J. Grant, K.E. Porter, M.T. Kearney, S.B. Wheatcroft, Increasing circulating IGFBP1 levels improves insulin sensitivity, promotes nitric oxide production, lowers blood pressure, and protects against atherosclerosis, Diabetes 61 (2012) 915–924.
[31] Z. Bibi, Role of cytochrome P450 in drug interactions, Nutr. Metab. 5 (2008) 27.
[32] L. Knockaert, B. Fromenty, M.A. Robin, Mechanisms of mitochondrial targeting of cytochrome P450 2E1: physiopathological role in liver injury and obesity, FEBS J. 278 (2011) 4252–4260.
[33] Y.-Y. Zhang, L. Yang, Interactions between human cytochrome P450 enzymes and steroids: physiological and pharmacological implications, Expet Opin. Drug Metabol. Toxicol. 5 (2009) 621–629.
[34] U. Weyemi, C. Dupuy, The emerging role of ROS-generating NADPH oxidase NOX4 in DNA-damage responses, Mutat. Res. Rev. Mutat. Res. 751 (2012) 77–81.
[35] E.G. Hrycay, S.M. Bandiera, Chapter two - involvement of cytochrome P450 in reactive oxygen species formation and cancer, in: J.P. Hardwick (Ed.), Advances in Pharmacology, Academic Press, 2015, pp. 35–84.
[36] S.H. Caldwell, L.A. De Freitas, S.H. Park, M.L. Moreno, J.A. Redick, C.A. Davis, B.J. Sisson, J.T. Patrie, H. Cotrim, C.K. Argo, A. Al-Osaimi, Intramitochondrial crystalline inclusions in nonalcoholic steatohepatitis, Hepatology 49 (2009) 1888–1895.
[37] S.H. Caldwell, R.H. Swerdlow, E.M. Khan, J.C. Iezzoni, E.E. Hespenheide, J.K. Parks, W.D. Parker Jr., Mitochondrial abnormalities in non-alcoholic steatohepatitis, J. Hepatol. 31 (1999) 430–434.
[38] C.J. Pirola, T.F. Gianotti, A.L. Burgueno, M. Rey-Funes, C.F. Loidl, P. Mallardi, J.S. Martino, G.O. Castano, S. Sookoian, Epigenetic modification of liver mitochondrial DNA is associated with histological severity of nonalcoholic fatty liver disease, Gut 62 (2013) 1356–1363.
[39] A.J. Sanyal, C. Campbell-Sargent, F. Mirshahi, W.B. Rizzo, M.J. Contos, R.K. Sterling, V.A. Luketic, M.L. Shiffman, J.N. Clore, Nonalcoholic steatohepatitis: association of insulin resistance and mitochondrial abnormalities, Gastroenterology 120 (2001) 1183–1192.
[40] D.C. Chan, Mitochondrial dynamics and its involvement in disease, Annu. Rev. Pathol. 15 (2020) 235–259.
[41] M. Giacomello, A. Pyakurel, C. Glytsou, L. Scorrano, The cell biology of mitochondrial membrane dynamics, Nat. Rev. Mol. Cell Biol. 21 (2020) 204–224.
[42] L. Pernas, L. Scorrano, Mito-morphosis: mitochondrial fusion, fission, and cristae remodeling as key mediators of cellular function, Annu. Rev. Physiol. 78 (2016) 505–531.
[43] H. Chen, S. Ren, C. Clish, M. Jain, V. Mootha, J.M. Mccaffery, D.C. Chan, Titration of mitochondrial fusion rescues Mff-deficient cardiomyopathy, J. Cell Biol. 211 (2015) 795–805.
[44] H. Chen, S.A. Detmer, A.J. Ewald, E.E. Griffin, S.E. Fraser, D.C. Chan, Mitofusins Mfn1 and Mfn2 coordinately regulate mitochondrial fusion and are essential for embryonic development, J. Cell Biol. 160 (2003) 189–200.
[45] T. Koshiba, S.A. Detmer, J.T. Kaiser, H. Chen, J.M. Mccaffery, D.C. Chan, Structural basis of mitochondrial tethering by mitofusin complexes, Science 305 (2004) 858–862.
[46] N. Ishihara, Y. Eura, K. Mihara, Mitofusin 1 and 2 play distinct roles in mitochondrial fusion reactions via GTPase activity, J. Cell Sci. 117 (2004) 6535–6546.
[47] O.M. De Brito, L. Scorrano, Mitofusin 2 tethers endoplasmic reticulum to mitochondria, Nature 456 (2008) 605–610.
[48] J.A. Mears, L.L. Lackner, S. Fang, E. Ingerman, J. Nunnari, J.E. Hinshaw, Conformational changes in Dnm1 support a contractile mechanism for mitochondrial fission, Nat. Struct. Mol. Biol. 18 (2011) 20–26.
[49] M.A. Karren, E.M. Coonrod, T.K. Anderson, J.M. Shaw, The role of Fis1p-Mdv1p interactions in mitochondrial fission complex assembly, J. Cell Biol. 171 (2005) 291–301.
[50] H. Otera, C. Wang, M.M. Cleland, K. Setoguchi, S. Yokota, R.J. Youle, K. Mihara, Mff is an essential factor for mitochondrial recruitment of Drp1 during mitochondrial fission in mammalian cells, J. Cell Biol. 191 (2010) 1141–1158.
[51] Y. Krishnasamy, M. Gooz, L. Li, J.J. Lemasters, Z. Zhong, Role of mitochondrial depolarization and disrupted mitochondrial homeostasis in non-alcoholic steatohepatitis and fibrosis in mice, Int J Physiol Pathophysiol Pharmacol 11 (2019) 190–204.
[52] T. Yamada, D. Murata, Y. Adachi, K. Itoh, S. Kameoka, A. Igarashi, T. Kato, Y. Araki, R.L. Huganir, T.M. Dawson, T. Yanagawa, K. Okamoto, M. Iijima, H. Sesaki, Mitochondrial stasis reveals p62-mediated ubiquitination in parkin-independent mitophagy and mitigates nonalcoholic fatty liver disease, Cell Metabol. 28 (2018) 588–604 e585.
[53] G. Twig, A. Elorza, A.J. Molina, H. Mohamed, J.D. Wikstrom, G. Walzer, L. Stiles, S.E. Haigh, S. Katz, G. Las, J. Alroy, M. Wu, B.F. Py, J. Yuan, J.T. Deeney, B. E. Corkey, O.S. Shirihai, Fission and selective fusion govern mitochondrial segregation and elimination by autophagy, EMBO J. 27 (2008) 433–446.
[54] G. Twig, O.S. Shirihai, The interplay between mitochondrial dynamics and mitophagy, Antioxidants Redox Signal. 14 (2011) 1939–1951.
[55] C.-Y. Liu, C.-J. Tsai, S. Yasugaki, N. Nagata, M. Morita, A. Isotani, M. Yanagisawa, Y. Hayashi, Copine-7 is required for REM sleep regulation following cage change or water immersion and restraint stress in mice, Neurosci. Res. 165 (2021) 14–25.
[56] M. Sekiya, A. Hiraishi, M. Touyama, K. Sakamoto, Oxidative stress induced lipid accumulation via SREBP1c activation in HepG2 cells, Biochem. Biophys. Res. Commun. 375 (2008) 602–607.
[57] A.K. Hauck, D.A. Bernlohr, Oxidative stress and lipotoxicity, J. Lipid Res. 57 (2016) 1976–1986.
[58] P. Newsholme, V.F. Cruzat, K.N. Keane, R. Carlessi, P.I. De Bittencourt Jr., Molecular mechanisms of ROS production and oxidative stress in diabetes, Biochem. J. 473 (2016) 4527–4550.